

Final Draft
of the original manuscript:

Li, W.; Chu, Q.; Yang, X.; Shen, J.; Vairis, A.; Wang, W.:
**Microstructure and morphology evolution of probeless friction stir spot
welded joints of aluminum alloy**
In: Journal of Materials Processing Technology. Vol. 252 (2020). 69 -80.
First published online by Elsevier: September 05, 2017

DOI: 10.1016/j.jmatprotec.2017.09.003
<https://dx.doi.org/10.1016/j.jmatprotec.2017.09.003>

Microstructure and mechanical optimization of probeless friction stir spot welded joint of an Al-Li alloy

Q. Chu¹, W.Y. Li^{1,*}, X.W. Yang¹, J.J. Shen², A. Vairis³, W.Y. Feng¹, W.B. Wang⁴

¹State Key Laboratory of Solidification Processing, Shaanxi Key Laboratory of Friction Welding Technologies, Northwestern Polytechnical University, Xi'an 710072, Shaanxi, P.R. China

²Helmholtz-Zentrum Geesthacht, Institute of Materials Research, Materials Mechanics, Geesthacht 21502, Germany

³Mechanical Engineering Department, TEI of Crete, Heraklion, Crete 71004, Greece

⁴China FSW Center, Beijing 100024, PR China

* Corresponding author. Tel.: ++86-29-88495226, Fax: ++86-29-88492642, E-mail:

liwy@nwpu.edu.cn (W.Y. Li)

Abstract

In this work, a third generation Al-Li alloy has been successfully spot welded with probeless friction stir spot welding (P-FSSW), which is a variant of conventional friction stir welding. The Box-Behnken experimental design in response surface methodology (RSM) was applied to optimize the P-FSSW parameters to attain maximum tensile/shear strength of the spot joints. Results show that an optimal failure load of 7.83 kN was obtained under a dwell time of 7.2 s, rotation speed of 950 rpm and plunge rate of 30 mm/min. Sufficient dwell time is essential for heat

conduction, material flow and expansion of the stir zone to form a sound joint. Two fracture modes were observed which were significantly affected by hook defect. In addition to mechanical testing, electron backscattering diffraction (EBSD) and differential scanning calorimetry (DSC) were used for microstructure evolution and property analysis. The precipitation of GP zone and Al_3Li assisted with the ultrafine grains were responsible for the high microhardness in the stir zone.

Keywords: Probeless friction stir spot welding; Precipitation; Mechanical property; Fracture mechanism

1. Introduction

The increasing use of Al-Li alloys offers a potential for substantial weight-saving in structural components to the aerospace industry ^[1,2]. The new generation Al-Li alloys have outstanding properties compared to typical Al alloys, such as low density, high specific strength and excellent corrosion resistance ^[3,4]. Furthermore, Al-Li alloys contain a wide variety of precipitates, depending on the heat treatment conditions selected, which usually include Guinier-Preston (GP) zones, T_1 (Al_2CuLi), θ' (Al_2Cu), β' (Al_3Zr), δ' (Al_3Li), and S' (Al_2CuMg), the reason for excellent mechanical properties ^[5].

The main problems of traditional fusion welding of Al-Li alloys are porosity, hot cracks and the loss of Li element ^[6]. Friction stir welding (FSW) is an innovative solid-state joining technology which is free of defects commonly associated with fusion welding ^[7]. As a variant of FSW, friction stir spot welding (FSSW) has been

applied to the spot joining in light alloys. In order to eliminate the keyhole inherent to FSSW joints, refill FSSW (RFSSW) and probeless FSSW (P-FSSW) have been proposed. Due to equipment complexity, the application of RFSSW is limited, while P-FSSW is a more simple process which produces welds of good finish [8].

Although both methods eliminate the keyhole, the hook defect can still be found in the joints, which is formed due to the flow of the heated and softened material [9]. Yin et al. [10] found that the beneficial effect of an increasing bond width on failure load is outweighed by a shape change of the hook defect. Similarly, Rosendo et al. [11] associated hook sharpness with the mode of fracture which reduced the joint mechanical strength. Cao et al. [12] indicated that the tensile/shear strength decreased monotonically with hook height, which had a positive correlation with welding parameters. Thus, friction stir spot brazing (FSSB) [13] and FSSW-FSW [14] were proposed to eliminate the hook defect. However, the addition of a metal interlayer or modification of the process added to the complexity of the techniques.

In this study, the aim was to optimize the welding process of P-FSSW and investigate the hook defect. To predict the mechanical strength of the joints, the Box-Behnken mathematical model in response surface methodology (RSM) was used. In addition to mechanical testing, differential scanning calorimetry (DSC) was also used for property and microstructure analysis.

2. Experimental

The material used in the experiment was AA 2198-T8 Al-Li alloy with a thickness

of 1.8 mm, which was degreased prior to welding. The schematic illustration of P-FSSW is shown in [Fig. 1](#). A probeless cylindrical tool with the shoulder diameter (D) of 15 mm was used which was made of H13, with three involute grooves machined on the shoulder surface.

A three-level and three-factorial Box-Behnken experimental design was used to study the dependence of failure load on parameters and optimize the weld process. The selected welding parameters and their levels are shown in [Table 1](#). The P-FSSW experiments were designed according to [Table 2](#). Note that the middle level value of rotation speed was set to 950 rpm instead of 965 rpm due to machine capability.

Samples for morphology analysis were etched using Keller's Reagent (2 ml HF, 3 ml HCl, 5 ml HNO₃, and 190 ml H₂O), and examined by optical microscopy (OM). For the tensile/shear tests, specimens were produced using two 65 mm×30 mm coupons with an overlap length of 30 mm and the tests were carried out in triplicate for each welding parameter at a head cross speed of 1mm/min at room temperature. Then the fracture features of the samples were analyzed by scanning electron microscopy (SEM).

Microhardness was measured across the cross section of the weld zone under a load of 0.2 kg. In addition to mechanical testing, the dissolution and precipitation behaviors of different regions of the weld were investigated with differential scanning calorimetry (DSC). The sample for DSC analyses was 3 mm in diameter with an average weight of 15 mg. The heating rate was 10 K/min and the heating temperature ranged from 293 K to 820 K. Results were corrected for baseline and normalized for

the sample weight.

3. Results and discussion

3.1 Microstructure

Fig. 2a shows the macrograph of the cross-section of a typical P-FSSWed joint made at the rotation speed of 950 rpm and dwell time of 6 s. The cross-section shows a typical asymmetrical 'basin' shape, which is divided into three regions: the stir zone (SZ), the thermo-mechanically affected zone (TMAZ) and the heat affected zone (HAZ) due to the difference in the plastic deformation and temperature during the P-FSSW process. The HAZ shows similar grain morphology to the base material which appears to be flattened and elongated due to thermal diffusion during welding process (Fig. 2b). During the P-FSSW process, a softened layer was formed in the SZ due to friction heat with the contact and penetration of shoulder. Subsequently, intense deformation and plastic flow occurred in the softened layer, resulting in the break-up of original grains. Due to the high temperature and intense deformation, refined and equiaxed grains formed within the SZ due to dynamic recrystallization (Fig. 2c). In a similar manner, the material in TMAZ was under severe friction heat and plastic deformation during welding. The microstructure in TMAZ was partially recrystallized, leading to highly deformed grains (Fig. 2d) with fine grains on the boundary. The deformed grains were bent and elongated upwards due to material flow ^[15].

A geometric defect like the hook can also be seen in Fig. 2a, which has an inverted 'V' shape. As the stir zone deepens, the upward material flow of the bottom sheet

occurs markedly. As a result, the boundary between the two sheets bends upward and the hook defect changes from obtuse to acute finally (Fig. 3). Campanelli et al. [16] found that the hook acts as a stress concentration region, especially when the interface deforms severely, providing a potential path for the initiation and even propagation of crack when the joint is subjected to an external load applied perpendicularly to the defect. Rosendo et al. [17] associated hook sharpness with the mode of fracture and found it responsible for the deterioration of the joint mechanical strength. In order to understand the effects of the morphologies of stir zone and hook defect on mechanical strength, the stir zone depth (SZD) and effective thickness of top sheet (EST, as defined in Fig. 3) were calculated.

Fig. 4 shows the changes of stir zone depth, effective sheet thickness and tensile/shear strength (TSS) with process parameters. With the increase of dwell time, SZD and EST change monotonically while TSS increases initially and then decreases. When the dwell time is set to a low value, TSS and SZD show the same trend. Due to limited heat input, the metals are insufficiently plasticized with limited material flow, making the stir zone depth low and not deforming the interface adequately, producing a poor joint. With the increase of dwell time, the material flow and deformation improve with sufficient heat input, which expands the stir zone and creates improved joints. At the same time, the hook defect is formed due to upward bending of the interface, supported by Chen et al. [18] who attributed the change in the morphology of hook defect to material flow, deformation and break-up of oxide film. In reality, as the stir zone expands, material next the stir zone edge is pushed outwards and upwards

due to compressive stresses which develop normally to the stir zone edge. In effect, the hook defect is forced further away from the axis of the tool and extends upwards with longer dwell times, resulting in rapid decrease of EST. Since the hook defect works as a crack nucleation site, a crack can nucleate and grow in the top sheet under small loads. Although SZD decreases due to the ejection of plasticized material when the heat input is overhigh, the TSS increases at the same time due to the restraint of hook defect. Therefore, the mechanical strength depends on the stir zone depth initially, but is controlled by the effective thickness of the top sheet once the hook defect extends appreciably.

3.2 DSC analysis

In order to study the precipitation kinetics in the weld, the DSC of samples from the SZ and HAZ in as-welded condition were carried out (Fig. 5). During the DSC, precipitation of phases is identified by the exothermic heat flow and endothermic reactions are due to dissolution of phases [19-21]. The area under the peak indicates the intensity of the precipitation or dissolution and the temperature at which it occurs is related to the thermal stability of that phase [22-24].

Several endothermic and exothermic events were identified from the DSC results. Endothermic peak labeled as A is due to the dissolution of GP zones formed during cooling process. Peak B is due to the dissolution of metastable δ' (Al_3Li) precipitate and it was found to be around 210 °C [19]. The exothermic peak C is due to the precipitation of T_1 (Al_2CuLi) phase (260 °C). And peak D is a large endothermic peak which is the dissolution of T_1 and other high temperature phase formed. Less than 1%

Li content in the third generation Al-Cu-Li alloys suppresses the formation of δ' precipitate [20], which explains the small amount of δ' dissolution. Decreus et al. [21] and Sidhar et al. [23] investigated the effect of the Cu/Li ratio on the precipitations in Al-Cu-Li alloys and found that Cu-rich clusters formed mostly in the Li-lean alloy, similarly δ' (Al_3Li) phase in Li-rich alloy. Also, Deschamps et al. [24] found a secondary precipitation peak between 300 and 350 C due to the thickening of T_1 phase, which is not pronounced in our results (Fig. 5a). When compared to the precipitation in the SZ, there is no endothermic peak corresponding to the dissolution of δ' (Al_3Li) in HAZ, possibly due to no or very limited δ' (Al_3Li) forming during welding (Fig. 5b).

The distribution of precipitates in different regions of the P-FSSWed joint is affected by friction heat and shear stress [25]. During welding, excessive friction heat generated in the SZ due to shoulder contact leads to the dissolution of the original phases (e.g. T_1 , θ'), which in turn increase the concentration of Li atoms in the matrix. Meanwhile, high strain energy, which can increase the driving force for δ' precipitation, was introduced into this zone by intense shear deformation [26]. As a consequence, rapid cooling of SZ resulted in the precipitation of δ' phase after welding. Compared to SZ, the phase T_1 did not dissolved but coarsened in the HAZ due to lower temperature during welding, resulting in the absence of precipitation of δ' phase.

3.3 Microhardness

Fig. 6b shows the two-dimensional distribution of Vickers micro hardness (HV)

after P-FSSW from the area with the border in the red in Fig. 6a. Hardness distribution indicates inhomogeneous microstructure developed across the joint [27]. Based on the distribution, there is a symmetrical “basin” shape, following that of the joint macrostructure. Overall hardness of the as-extruded AA2198 alloys was 155-165 HV. In the BM, T_1 (Al_2CuLi) phase is the main strengthening precipitation, which nucleates most efficiently on dislocation by reducing the strain energy, indicated by Malard et al. [28]. Closer to the stir zone, increased temperature due to friction heat results in coarsening or dissolution of precipitates, which softens the material.

The largest hardness drop was observed in the HAZ in age-hardened aluminum alloys, related to the coarsening of precipitates [29]. Hardness values in the HAZ ranged from 100HV to 108HV, because of the recovery of BM as the temperature in this region is moderate during welding. However, severe deformation in the TMAZ produces limited strain hardening, which in turn suppresses the softening.

In the SZ, hardness approximately reaches 112HV, which is higher than that of HAZ. As the Hall-Petch formula indicates, hardness is inversely proportional to the grain size. Thus, fine equiaxed grains formed due to dynamic recrystallization, the result of sufficient temperature and plastic deformation, lead to high hardness values in the SZ. At the same time, a variety of {Cu, Li} solute atoms is expected in the Al matrix because of the dissolution of {Al, Cu, Li} precipitates in the SZ. This forms the GP zone and Al_3Li phase, as the DSC measurements show. It should be noted that there is local hardness maximum around the center of the SZ due to the extrusion resulting from local material flow and axial force.

3.4 Optimizing the welding process

3.4.1 Tensile/shear strength of P-FSSWed joints

During the tensile/shear test, the Box-Behnken mathematical model was used to study the dependence of failure load on parameters and optimize the weld process. The response, i.e. the tensile/shear strength (TSS), is a function of the welding parameters such as dwell time (DT), plunge rate (PR) and rotation speed (RS), and it can be expressed as

$$\text{TSS} = f(\text{DT}, \text{PR}, \text{RS})$$

The multiple regression equation used to represent the response surface Y is given by

$$Y = a_0 + \sum a_i x_i + \sum a_{ii} x_i^2 + \sum a_{ij} x_i x_j$$

where a_0 is the average of the responses and a_i , a_{ii} , a_{ij} are the regression coefficients ^[30] that depend on respective linear, squared and interactive terms of parameters. The values of the coefficients were calculated using the Design Expert Software.

$$\begin{aligned} \text{TSS} = & -37.66512 + 0.058810 \text{ RS} + 4.80601 \text{ DT} - 0.064667 \text{ PR} - 4.00775\text{E-}004 \text{ RS} \times \\ & \text{DT} + 1.88779\text{E-}004 \text{ RS} \times \text{PR} + 7.81250\text{E-}003 \text{ DT} \times \text{PR} - 3.11455\text{E-}005 \text{ RS}^2 - \\ & 0.32508 \text{ DT}^2 - 2.74612\text{E-}003 \text{ PR}^2 \end{aligned}$$

The analysis of variance (ANOVA) technique was used to check the adequacy of the developed empirical relationship. The significance of each coefficient was determined by p values, shown in [Table 3](#). Values of p under 0.05 indicate a significant terms. Values over 0.10 indicate the opposite. In this case, DT, RS², DT² are significant terms, followed by PR² and RS-PR.

The very low probability value ($\text{Prob} > F = 0.0018$) indicates a very high significance for the regression model. The fitness of the model is checked by the determination coefficient (R^2). The adjusted determination coefficient (adjusted- R^2) is 0.8592, indicating the compatibility with the data predicted by the model.

In order to visually study the effects of the parameters on the mechanical strength and obtain the optimum parameters of the welding process, 3D response graphs are shown in Fig. 7. The apex of the response graph shows the maximum achievable TSS. It is clear from Fig. 7 that the TSS increases with dwell time and rotation speed to a maximum as there is increased heat input and sufficient material flow, and then decreases due to the hook defect. The plunge rate does not affect significantly the tensile/shear strength of the P-FSSWed joints. In addition, when the dwell time is short, the strength of P-FSSWed joint is still poor even though the rotation speed is raised (Fig. 7a). Although peak temperature can be achieved in a short time with rotation speed, the heat input may not increase due to the short dwell time. A sufficiently long dwell time is essential for heat conduction, material flow and expansion of the stir zone to form a sound joint. When the dwell time and rotation speed have low values, the detrimental effect of plunge rate on tensile/shear strength is more pronounced (Figs. 7b and 7c). Due to insufficient heat input, the materials are hard to be plasticized, which are extruded out of the stir zone during the plunge stage, leading to a poor joint.

From the response surface graphs, it can be seen that the maximum tensile/shear failure is 7.83 kN. The corresponding parameters for this maximum are a dwell time

of 7.2 s, a rotation speed of 950 rpm and a plunge rate of 30 mm/min. To validate the results, a P-FSSW experiment was conducted using the optimum welding parameters. The experimental TSS result of 7.84 ± 0.42 kN is in very good agreement with the predicted value.

3.4.2 Fracture mode

From the fractured tensile/shear testing samples, two distinct fracture modes are observed for the spot weld, as shown in Fig. 8. In the first one, shear fracture (mode I, Fig. 8a) occurs and separates the two parts at the interface as cracks which extend along the initial interface of the spot weld between both sheets. As a result, the stir zone is removed from the joint and remains entirely attached to the top sheet. And in the second mode, plug fracture (mode II, Fig. 8b) occurs with cracks extending from the hook defect and propagating toward the surface of the top sheet along the edge of the stir zone. As a result, the stir zone is removed from the joint and remains entirely attached to the bottom sheet. This is also described as pull-out mode [31,32]. Based on the fracture morphologies, both fracture modes are associated to the same fracture mechanism in which the hook defect plays an important role. While the stir zone expands, material adjacent to the stir zone edge is pushed outwards and upwards, moving the hook defect in a similar manner. In effect, the failure location shifts further away from the interface (shear fracture) and moves towards the surface of the top sheet. Finally, fracture occurs at the hook defect in the top sheet (plug fracture).

Typical fractographs of the two fracture modes are shown in Figs. 8c-8f. Substantial material movement in the circumferential direction can be seen in Fig. 8a

(black round arrow), where the stir zone is extensive. Material flow is more pronounced at the outer parts of the stir zone as the red arrows indicate, due to an upward material flow in the bottom sheet, also noted in literature [33]. Close-up views of the selected region C in Fig. 8a show a number of elongated dimples in the bottom of the stir zone (Fig. 8c), indicating a sound joint. The region D is from the slope of the hook, and has fewer dimples compared to region C, indicating that the crack originates preferentially from region D (Fig. 8d). In the second case (Fig. 8b), there are tearing edges, flat facets, and few shallow dimples (red arrow) in regions E and F (Figs. 8e and 8f), indicating that the hook defect is a weak connection.

4. Conclusions

In this work, 1.8 mm thick AA2198 Al-Li alloy sheets were jointed using P-FSSW. The effect of welding parameters on the microstructure and the mechanical properties of the joints were investigated. The Box-Behnken experimental design method was used to investigate the effect of the welding parameters on the mechanical strength. The following conclusions can be drawn:

(1) The tensile/shear strength of P-FSSWed joints increases with the stir zone depth initially, thereafter it is mainly affected by hook defect. Due to the upward material flow of the bottom sheet, the hook defect extends appreciably and the effective thickness of the top sheet decreases rapidly, resulting in the decrease of the tensile/shear strength.

(2) The largest hardness drop was observed in the HAZ in age-hardened aluminum

alloys, which was related to the coarsening of precipitates. Increased hardness in SZ was associated with the formation of GP zone and Al_3Li phase accompanied by ultrafine grains.

(3) The Box-Behnken experimental design using the response surface methodology (RSM) was used to accurately predict the relation of the welding parameter and the tensile/shear properties of P-FSSWed joints. The optimum failure load of 7.83 kN was obtained for a dwell time of 7.2 s, rotation speed of 950 rpm and plunge rate of 30mm/min.

(4) The macrographs of failure samples reveal two distinct fracture modes, shear fracture and plug fracture. With the deterioration of hook defect, failure originates at the hook defect and shifts further away from the interface (shear fracture) towards the surface of top sheet (plug fracture).

Acknowledgement

The authors are grateful for the financial support of the National Natural Science Foundation of China [51574196], the Aviation Science Foundation [20161125002], and the 111 Project [B08040].

References

[1] H.Y. Li, D.S. Huang, W. Kang, J.J. Liu, Y.X. Ou, D.W. Li, J. Mater. Sci. Technol. 32 (2016) 1049-1053.

[2] Y. Tao, D.R. Ni, B.L. Xiao, Z.Y. Ma, W. Wu, R.X. Zhang, Y.S. Zeng, Mater. Sci.

- Eng. A 693 (2017) 1-13.
- [3] Q. Chu, X.W. Yang, W.Y. Li, Y.B. Li, *Sci. Technol. Weld. Joi.* 21 (2016) 164-170.
- [4] F.F. Wang, W.Y. Li, J. Shen, S.Y. Hu, J. dos Santos, *Mater. Design* 86 (2015) 933-940.
- [5] B. Decreus, A. Deschamps, F. De Geuser, P. Donnadieu, C. Sigli, M. Weyland, *Acta Mater.* 61 (2013) 2207-2218.
- [6] H.J. Liu, Y.Y. Hu, C. Dou, D.P. Sekulic, *Mater. Charact.* 123 (2017) 9-19.
- [7] Y. Yang, L.L. Zhou, *J. Mater. Sci. Technol.* 30 (2014) 1251-1254.
- [8] R.Z. Xu, D.R. Ni, Q. Yang, C.Z. Liu, Z.Y. Ma, *J. Mater. Sci. Technol.* 32 (2016) 76-88.
- [9] Q. Chu, W.Y. Li, X.W. Yang, J.J. Shen, Y.B. Li, W.B. Wang, *Weld. World* 61 (2017) 291-298.
- [10] Y.H. Yin, N. Sun, T.H. North, S.S. Hu, *J. Mater. Process. Technol.* 210 (2010) 2062-2070.
- [11] T. Rosendo, B. Parra, M.A.D. Tier, A.A.M.D. Silva, J.F.D. Santos, T.R. Strohaecker, *Mater. Design* 32 (2011) 1094-1100.
- [12] J.Y. Cao, M. Wang, L. Kong, L. J. Guo, *J. Mater. Process. Technol.* 230 (2016) 254-262.
- [13] R.Z. Xu, D.R. Ni, Q. Yang, C.Z. Liu, Z.Y. Ma, *Sci. Technol. Weld. Joi.* (2016) 1-8.
- [14] W.Y. Li, J.F. Li, Z.H. Zhang, D.L. Gao, W.B. Wang, C.L. Dong, *Mater. Design* 62 (2014) 247-254.

- [15] Z.L. Liu, H.T. Cui, S.D. Ji, M.Q. Xu, X.C. Meng, *J. Mater. Sci. Technol.* 32 (2016) 1372-1377.
- [16] L.C. Campanelli, U.F.H. Suhuddin, A.Í.S. Antonialli, J.F.D. Santos, N.G.D. Alcântara, C. Bolfarini, *J. Mater. Process. Technol.* 213 (2013) 515-521.
- [17] T. Rosendo, B. Parra, M.A.D. Tier, A.A.M.D. Silva, J.F.D. Santos, T.R. Strohaecker, *Mater. Design* 32 (2011) 1094-1100.
- [18] H. Chen, L. Fu, P. Liang, F. Liu, *Mater. Charact.* 125 (2017) 160-173.
- [19] B. Cai, Z. Zheng, D. He, S. Li, H. Li, *J. Alloys Compd.* 649 (2015) 19-27.
- [20] H. Sidhar, R.S. Mishra, *Mater. Design* 110 (2016) 60-71.
- [21] B. Decreus, A. Deschamps, F.D. Geuser, P. Donnadieu, C. Sigli, M. Weyland, *Acta Mater.* 61 (2013) 2207-2218.
- [22] C. Gao, Z.X. Zhu, J. Han, H.J. Li, *Mater. Sci. Eng. A* 639 (2015) 489-499.
- [23] H. Sidhar, N.Y. Martinez, R.S. Mishra, J. Silvanus, *Mater. Design* 106 (2016) 146-152.
- [24] A. Deschamps, M. Garcia, J. Chevy, B. Davo, F. De Geuser, *Acta Mater.* 122 (2017) 32-46.
- [25] Z.X. Zhu, J. Han, C. Gao, M. Liu, J.W. Song, Z.W. Wang, H.J. Li, *Mater. Sci. Eng. A* 681 (2017) 65-73.
- [26] Y. Lin, Z. Zheng, *Mater. Charact.* 123 (2017) 307-314.
- [27] I. Nikulin, S. Malopheyev, A. Kipelova, R. Kaibyshev, *Mater. Lett.* 66 (2012) 311-313.
- [28] B. Malard, F. De Geuser, A. Deschamps, *Acta Mater.* 101 (2015) 90-100.

- [29] J.H. Cho, H.H. Sang, G.L. Chang, *Mater. Lett.* 180 (2016) 157-161.
- [30] Z.W. Xu, Z.W. Li, S.D. Ji, L.G. Zhang, *J. Mater. Sci. Technol.* (2017).
- [31] Y. Tozakii, Y. Uematsu, K. Tokaji, *J. Mater. Process. Technol.* 210 (2010) 844-851.
- [32] W. Yuan, B. Carlson, R. Verma, R. Szymanski, *Sci. Technol. Weld. Joi.* 17 (2012) 375-380.
- [33] C. Gao, R.Q. Gao, Y. Ma, *Mater. Design* 83 (2015) 719-727.

Table and figure captions:

Table 1 Welding parameters and their levels.

Table 2 Box-Behnken design matrix.

Table 3 ANOVA test results.

Fig. 1. Schematic illustration of the P-FSSW process: (a) plunge stage, (b) dwell stage and (c) retract stage.

Fig. 2. (a) OM macrograph of cross section of P-FSSWed joint (950 rpm/6 s), the microstructure of (b) HAZ and (c) SZ and (d) TMAZ.

Fig. 3. Dependency of hook defect morphology on welding parameters: (a) 950 rpm/3 s, (b) 950 rpm/6 s, (c) 950 rpm/12 s and (d) 1180 rpm/12 s.

Fig. 4. Changes of stir zone depth, effective sheet thickness and tensile/shear strength with welding parameters.

Fig. 6. (a) Cross section of the P-FSSWed joint, and (b) hardness distribution corresponding to the area outlined in red in Fig. 6a.

Fig. 7. The effect of welding parameters on tensile/shear strength for (a) plunge rate of 30 mm/min, (b) rotation speed of 950 rpm and (c) dwell time of 6 s.

Fig. 8. Fractographs of the spot weld with different fracture modes in bottom sheets: (a) shear fracture (mode I), (b) plug fracture (mode II), (c) and (d) magnification of regions C and D in Fig. 8a, and (e) and (f) magnification of regions E and F in Fig. 8b.

Table 1 Welding parameters and their levels.

| Parameter | Notation | Level | | |
|----------------------|----------|----------|------------|----------|
| | | Low (-1) | Middle (0) | High (1) |
| Dwell time (s) | DT | 3 | 6 | 9 |
| Plunge rate (mm/min) | PR | 10 | 30 | 50 |
| Rotation speed (rpm) | RS | 750 | 965 (950) | 1180 |

Table 2 Box-Behnken design matrix.

| No. | RS (rpm) | DT (s) | PR (mm/min) |
|-----|----------|--------|----------------|
| 1 | 1180 | 9 | 30 |
| 2 | 1180 | 3 | 30 |
| 3 | 750 | 9 | 30 |
| 4 | 750 | 3 | 30 |
| 5 | 1180 | 6 | 50 |
| 6 | 1180 | 6 | 10 |
| 7 | 750 | 6 | 50 |
| 8 | 750 | 6 | 10 |
| 9 | 965 | 9 | 50 |
| 10 | 965 | 9 | 10 |
| 11 | 965 | 3 | 50 |
| 12 | 965 | 3 | 10 |
| 13 | 965 | 6 | 30 |
| 14 | 965 | 6 | 30 |
| 15 | 965 | 6 | 30 |
| 16 | 965 | 6 | 30 |
| 17 | 965 | 6 | 30 |

Table 3 ANOVA test results.

| Source | Sum of Squares | df | Mean Square | F Value | p-value Prob>F |
|-----------------|----------------|----|-------------|------------|----------------|
| Model | 100.37 | 9 | 11.15 | 11.85 | 0.0018 |
| RS | 1.42 | 1 | 1.42 | 1.51 | 0.2594 |
| DT | 40.79 | 1 | 40.79 | 43.35 | 0.0003 |
| PR | 4.805E-004 | 1 | 4.805E-004 | 5.106E-004 | 0.9826 |
| RS-DT | 0.27 | 1 | 0.27 | 0.28 | 0.6106 |
| RS-PR | 2.64 | 1 | 2.64 | 2.80 | 0.1381 |
| DT-PR | 0.88 | 1 | 0.88 | 0.93 | 0.3660 |
| RS ² | 8.73 | 1 | 8.73 | 9.27 | 0.0187 |
| DT ² | 36.04 | 1 | 36.04 | 38.30 | 0.0005 |
| PR ² | 5.08 | 1 | 5.08 | 5.40 | 0.0531 |
| Residual | 6.59 | 7 | 0.94 | | |
| Lack of Fit | 6.50 | 3 | 2.17 | 96.46 | 0.0003 |
| Pure Error | 0.090 | 4 | 0.022 | | |
| Cor Total | 106.96 | 16 | | | |

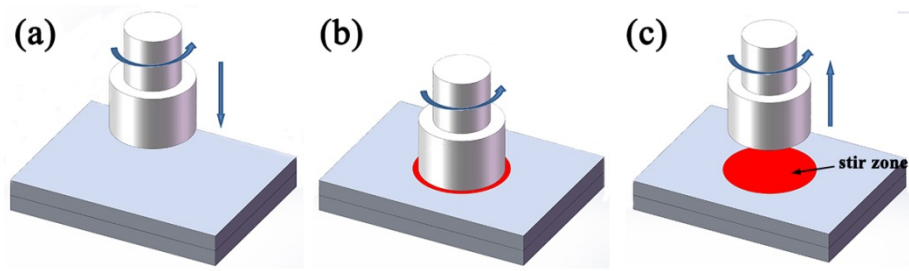


Fig. 1. Schematic illustration of the P-FSSW process: (a) plunge stage, (b) dwell stage and (c) retract stage.

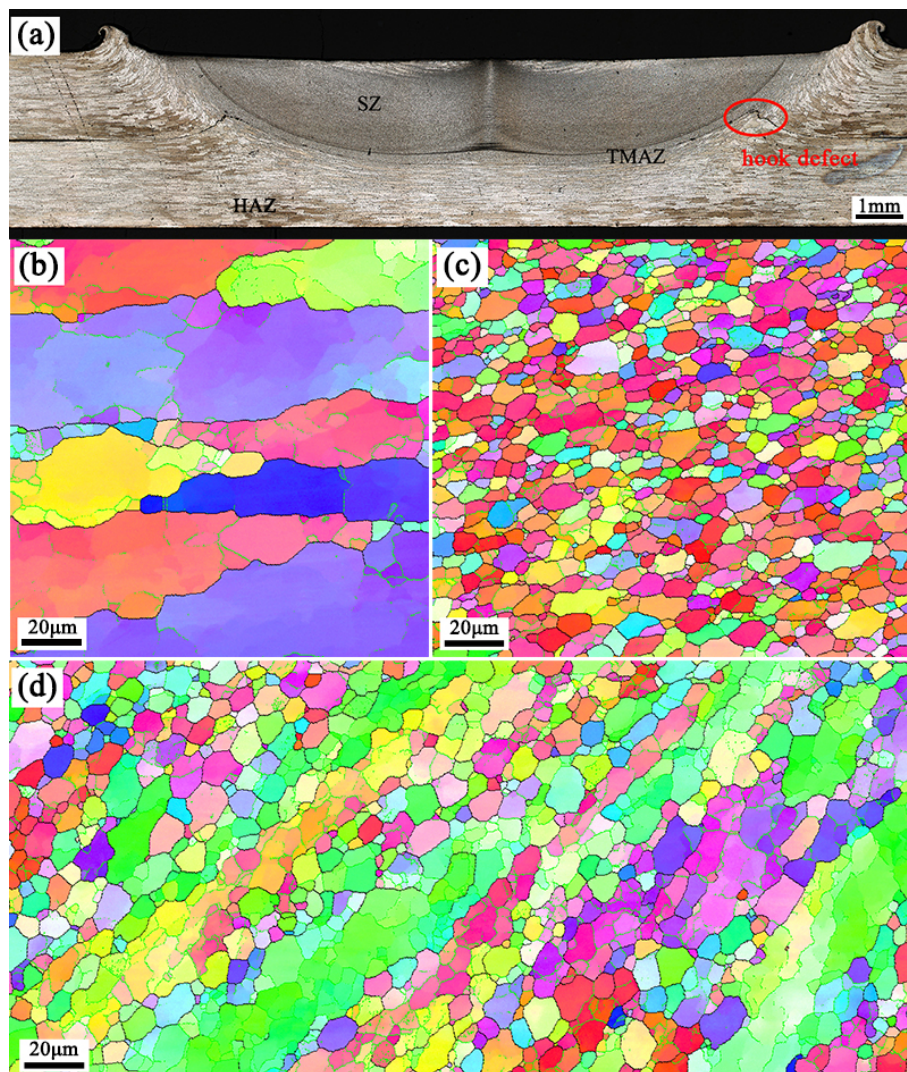


Fig. 2. (a) OM macrograph of cross section of P-FSSWed joint (950 rpm/6 s), the microstructure of (b) HAZ and (c) SZ and (d) TMAZ.

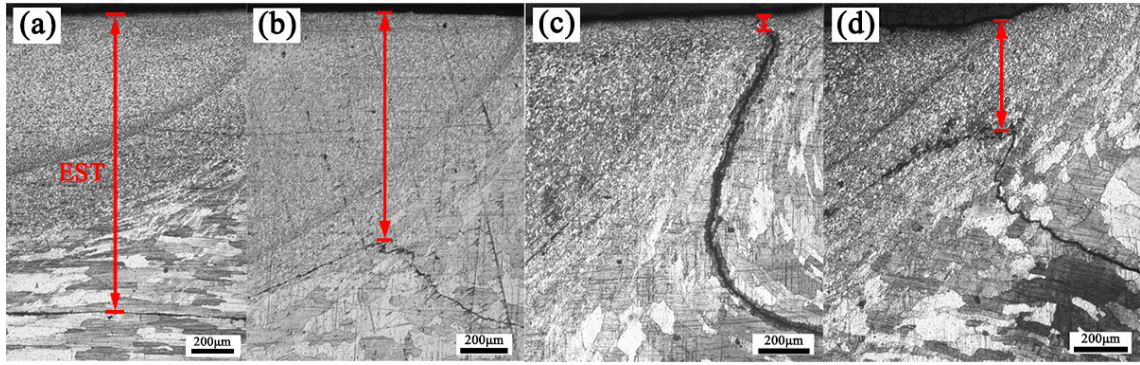


Fig. 3. Dependency of hook defect morphology on welding parameters: (a) 950 rpm/3 s, (b) 950 rpm/6 s, (c) 950 rpm/12 s and (d) 1180 rpm/12 s.

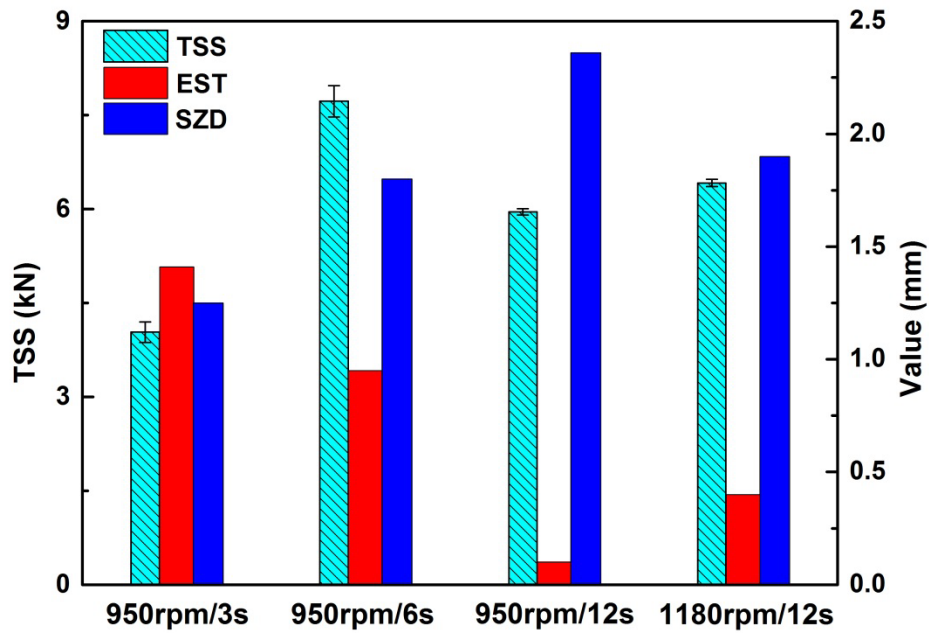


Fig. 4. Changes of stir zone depth, effective sheet thickness and tensile/shear strength with welding parameters.

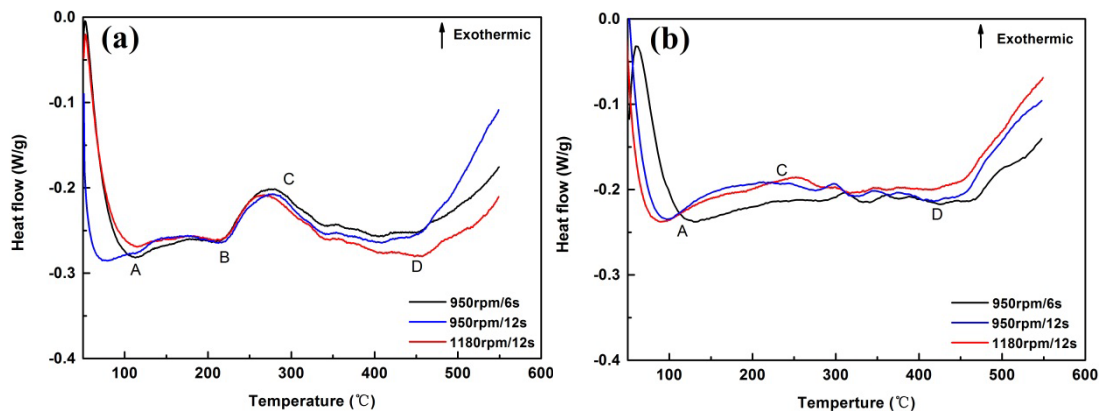


Fig. 5. DSC results for samples from (a) SZ and (b) HAZ for the as-welded condition.

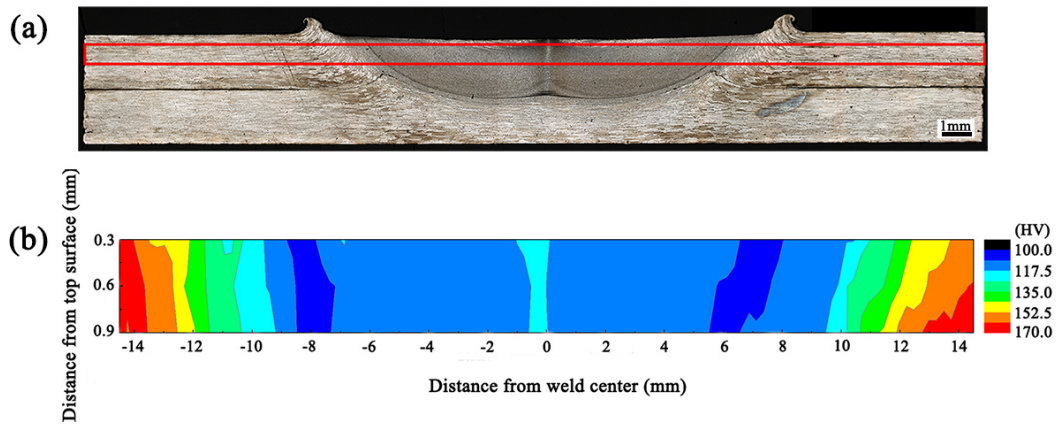


Fig. 6. (a) Cross section of the P-FSSWed joint, and (b) hardness distribution corresponding to the area outlined in red in Fig. 6a.

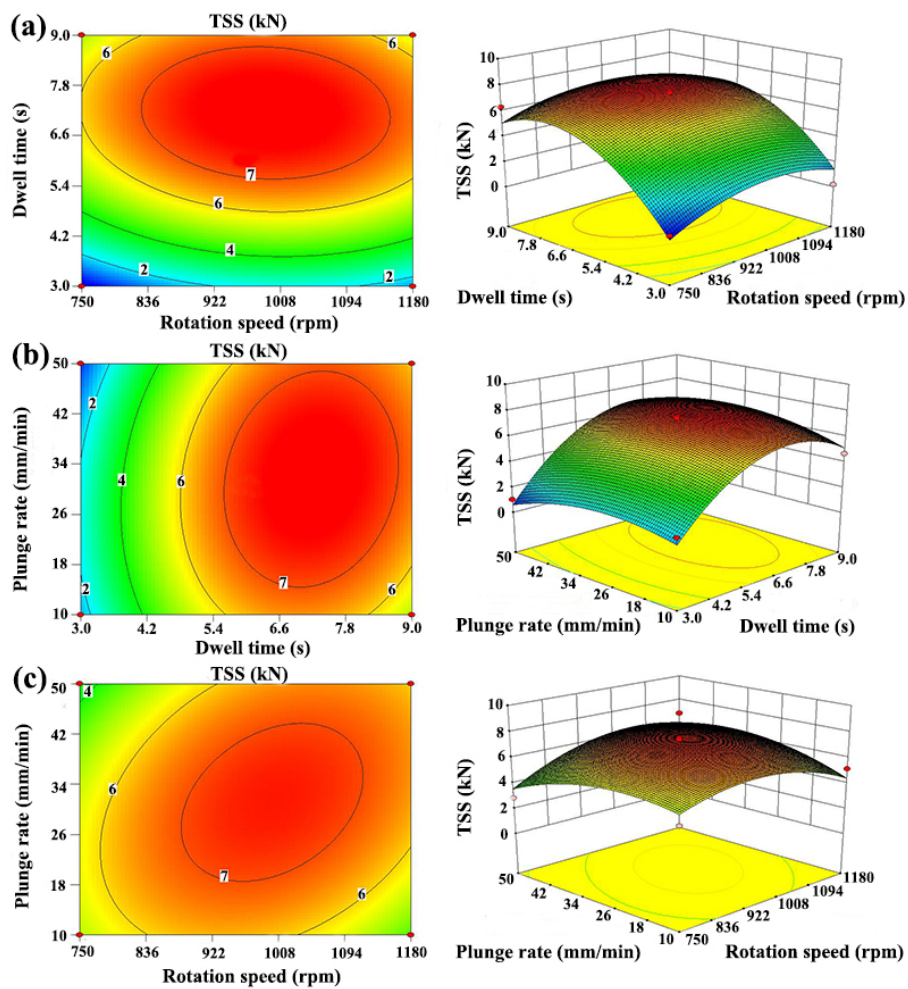


Fig. 7. The effect of welding parameters on tensile/shear strength for (a) plunge rate of 30 mm/min, (b) rotation speed of 950 rpm and (c) dwell time of 6 s.

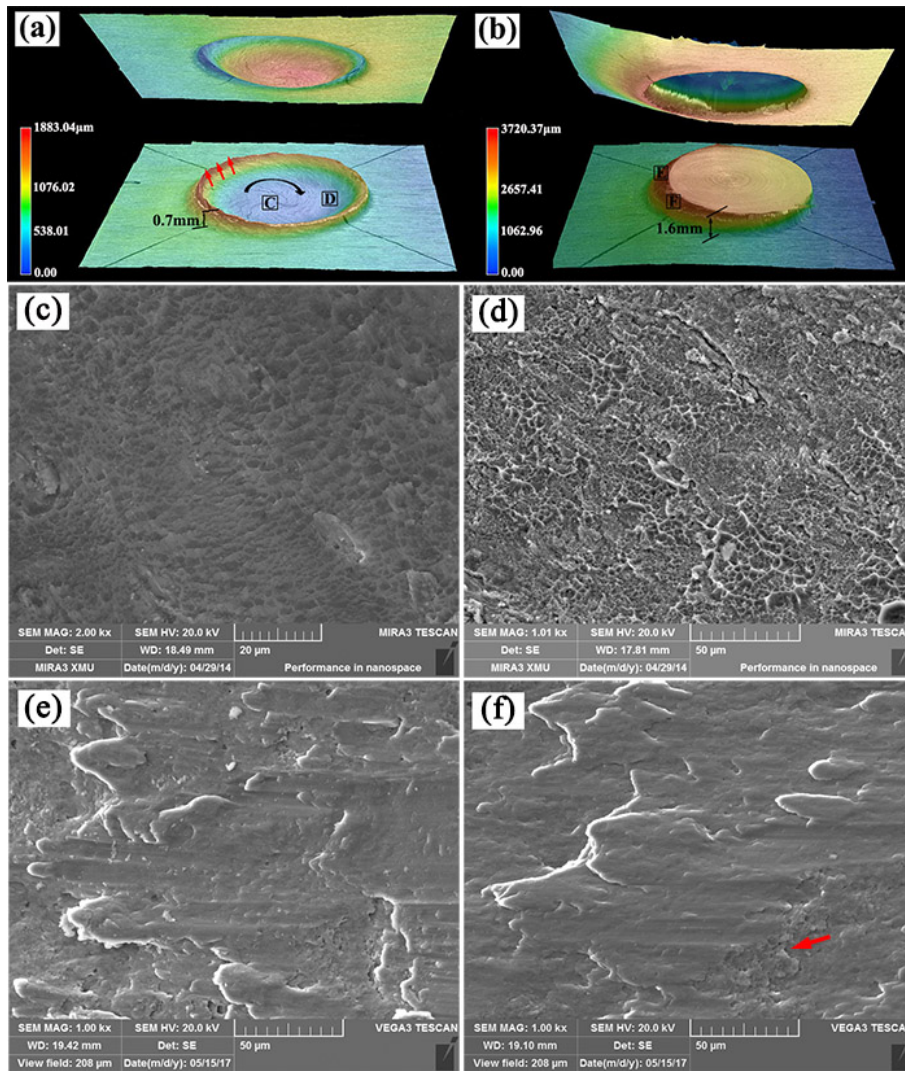


Fig. 8. Fractographs of the spot weld with different fracture modes in bottom sheets: (a) shear fracture (mode I), (b) plug fracture (mode II), (c) and (d) magnification of regions C and D in Fig. 8a, and (e) and (f) magnification of regions E and F in Fig. 8b.